SLAC-PUB-2647
November 1980
(E/I)

DRIFT AND PROPORTIONAL TRACKING CHAMBERS *

John A. Jaros
Stanford Linear Accelerator Center
Stanford University, Stanford, California 94305

Presented at the SLAC Summer Institute

Stanford Linear Accelerator Center

Stanford, California

July 28 - August 8, 1980

---

*Work supported by the Department of Energy, contract DE-AC03-76SF00515.

I. INTRODUCTION

Many techniques have been exploited in constructing tracking chambers, particle detectors which measure the trajectories and momenta of charged particles. The particular features of high-energy interactions — charged particle multiplicities, angular correlations and complex vertex topologies, to name a few — and the experimental environment of the accelerator — event rates, background rates, and so on — accent the importance of certain detector characteristics. In high energy e^+e^-, $\bar{p}p$ and pp interactions the final states are dominated by closely collimated jets of high multiplicity, requiring good track-pair resolution in the tracking chamber. High energy particles deflect very little in limited magnetic field volumes, necessitating good spatial resolution for accurate momentum measurements. The colliding beam technique generally requires a device easily adapted to full solid-angle coverage, and the high event rates expected in some of these machines put a premium on good time resolution. Finally, the production and subsequent decays of the tau, charmed and beautiful mesons will provide multiple vertex topologies. To reconstruct these vertices reliably will require considerable improvements in spatial resolution and track-pair resolution.

This lecture will consider the proportional counter and its descendant, the drift chamber, as tracking chambers. Its goal is to review the physics of this device in order to understand its performance limitations and promises. There are several excellent references on the physics of proportional and drift chambers; the reviews of Charpak,[1] Sauli,[2] and Sadoulet[3] have been especially valuable in preparing this lecture.

The proportional counter dates from 1908, when it was introduced by Geiger and Rutherford. It consists of a thin-walled cylinder with a fine wire on its axis. With an appropriate gas mixture and a high voltage applied between the wire and cylinder, the counter detects ionizing radiation by collecting and then amplifying the electrons left after the passage of the radiation through the gas. The recent popularity of the device derives from Charpak's invention of large multiple-anode wire structures which operate at sufficiently high gain that inexpensive electronics can be used to sense the deposited ionization. The evolution of the technique is shown schematically in Figure 1. Charpak's initial invention, the multi-wire proportional chamber, consists of a sandwich of cathode planes about a layer of fine anode wires (Figure 1(a)). The array serves as a proportional chamber hodoscope. It was recognized that the time between the passage of a charged particle and the appearance of the pulse on the anode wire, the drift time, is a measure of the location of the charged particle's trajectory. By including cathode wires in the anode plane to increase field gradients and demarcate cell boundaries (Figure 1(b)), the multi-wire proportional chamber was successfully adapted for drift time measurements. Figure 1(c) shows another variation of the drift chamber. Here the voltage applied to the main cathode layers is graded to create a nearly uniform collecting field, and thus a uniform electron drift velocity, throughout the cell. Figure 1(d) shows the individual drift-cell geometry common to several of the large solenoidal magnetic spectrometers at PEP and PETRA; and Figure 1(e) shows the "jet chamber" structure adopted for the Jade detector at PETRA. Here we will concentrate on the basic element of all these devices, the simple drift cell in the form of a cylindrical tube with an anode wire on its axis.

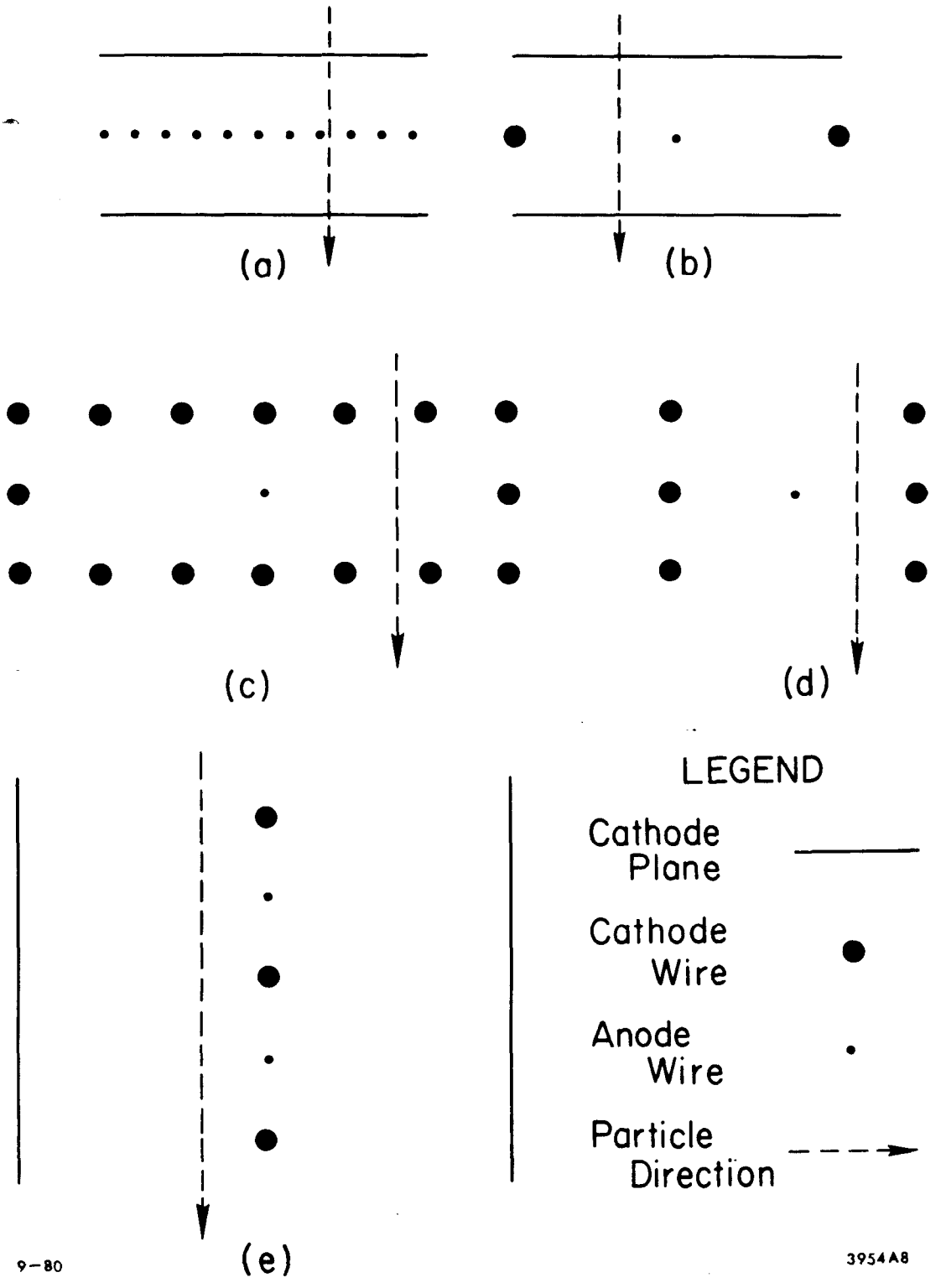

Fig. 1. Electrode arrangements in drift chambers. (a) the multi-wire proportional chamber; (b) planar drift chamber; (c) planar drift chamber with field shaping; (d) Mark II-style drift cell; (e) Jade-style jet chamber.

The plan of the lecture is as follows. We will follow the life history of the electrons released by the passage of a charged particle, reviewing the ionization process, drift and diffusion in electric and magnetic fields, amplification, and pulse formation. We will conclude by summarizing the fundamental limitations to drift chamber performance, especially to spatial resolution, since this is an area where practical improvements can be expected.

II. THE IONIZATION CHANNEL

Professor Ritson[4] has discussed how accurately the electrons ionized by the passage of a charged particle through a gas mark the trajectory of the particle. The picture which emerges is the following. In passing through 1 cm of argon gas at STP, a minimum ionizing particle undergoes about 30 ionizing collisions. Table 1 lists the ionization potentials and number of ionizing collisions for some of the other gases used in proportional chambers. The great majority of the collisions release a single electron with an effective range less than 1μ. Only about .2% of the collisions impart enough energy to the electrons to smear the track definition beyond 1 μ, and many of these δ-rays come to rest within 200 μ or so of the track. Thus the particle trajectory is delineated to the micron level by single electrons marking the collision locations. Only infrequently does a delta ray significantly degrade the resolution. In the organic gases commonly mixed with argon, the δ-ray situation should be even more benign. In any case, the spatial resolution limitations imposed by the ionization process are at the micron level and are well below limitations due to the other effects we shall consider.

The statistical nature of the ionization process already imposes limitations on the accuracy possible in a drift chamber. To study it, we consider a cylindrical proportional tube with a fine anode wire on

TABLE 1

GAS	IONIZATION POTENTIAL (eV)	NUMBER OF ION PAIRS (cm^{-1})
CO_2	13.7	34
CH_4	15.2	16
C_4H_{10}	10.6	46
Ne	21.5	12
Ar	15.7	29.4
Xe	12.1	44

the cylinder's axis. Let us also assume the electron drift velocity is a constant, independent of the distance from the anode. This will accurately approximate the behavior of most chambers near the anode wire.

Consider a track passing the anode wire with an impact parameter b; n electrons per centimeter are distributed along this track. (See Figure 2.) If the electronics is sensitive to the arrival of the first electron, the drift time measures the distance to the electron nearest the anode wire. This distance, ℓ, varies from event to event because of the statistical nature of the ionization process. The probability density for finding the first electron a distance y along the track from the point of closest approach is Poissonian:

$$P(y) = 2ne^{-2ny} \tag{1}$$

The dispersion in the distance to the anode wire follows and is given by

$$\sigma_e = \sqrt{\frac{5}{16}} \frac{1}{n^2 b} \tag{2}$$

in the limit where $b >> 1/n$. The ionization statistics thus limit the accuracy of drift-time measurements. In practice, these limitations are only important within 1 mm or so of the anode and cathode wires in a typical drift chamber. Figure 3 shows the limiting resolution as a function of the track's impact parameter for the cases $n = 30\ cm^{-1}$ and $n = 60\ cm^{-1}$. Increasing the density of ionization clusters by increasing the pressure or by choosing a gas with large n improves the resolution.

The results above apply to the common situation where the electronics is sensitive to the arrival of the first electron. Other detection

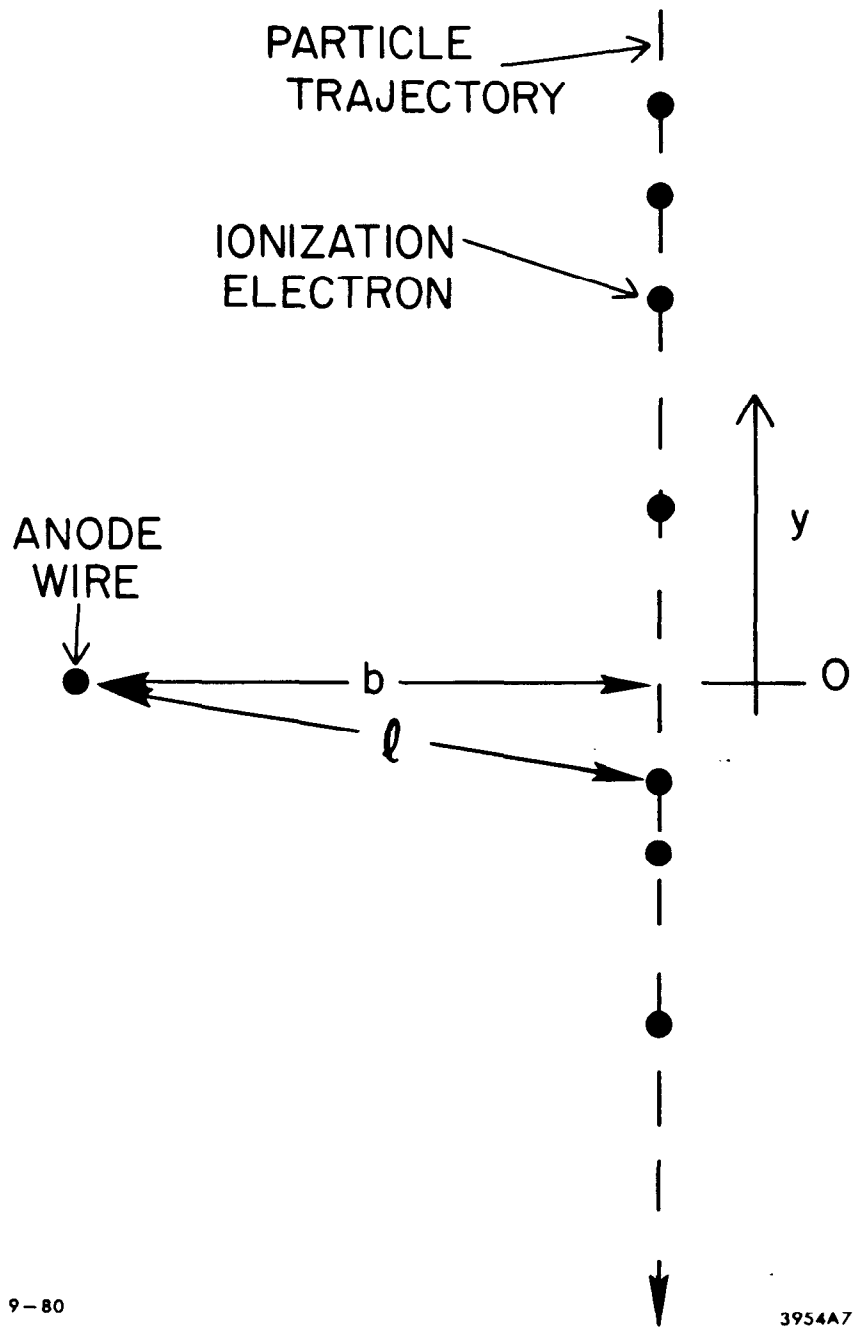

Fig. 2. Ionization deposited in a drift cell.

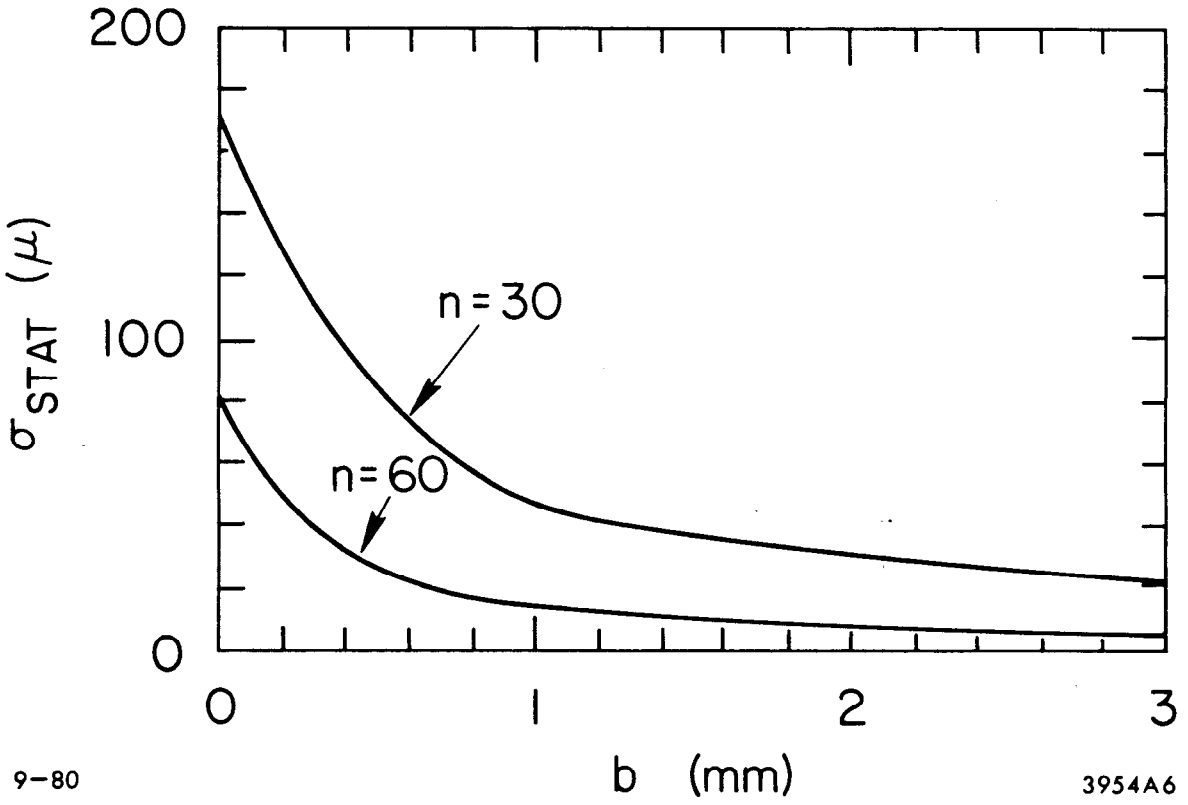

Fig. 3. Spatial resolution due to ionization statistics vs. impact parameter.

strategies are possible and may be desirable, especially in the case of long drift distances.

III. ELECTRON COLLECTION

The electrode structures we have considered in Figure 1 typically provide electric fields in the 1 kV/cm range throughout most of the active area of the drift cell, increasing inversely with the radius near the anode wire. The response of the electrons to these fields is two-fold. First, the electron temperature increases from typical thermal levels to the .1 - 1 eV range, depending on the gas and field strength, with the distribution of electron energies becoming decidedly non-Maxwellian. Second, a slow drift along the field lines toward the anode is imposed on the random thermal motion of the electrons. This drift velocity is an order of magnitude slower than the average thermal velocity of the electrons.

Classical statistical mechanics gives a good description of electron drift in electric fields. Palladino and Sadoulet[3] have applied these methods to the study of drift chamber gases. Reference 2 gives the electron energy distribution, $F(\varepsilon)$, in terms of the field strength E, the mean free path $\lambda(\varepsilon)$, and the fraction of energy lost per collision $\Lambda(\varepsilon)$, as

$$F(\varepsilon) = C\sqrt{\varepsilon}\, \exp\left\{ - \int \frac{3\Lambda(\varepsilon)\varepsilon d\varepsilon}{[eE\lambda(\varepsilon)]^2 + 3\varepsilon kT\Lambda(\varepsilon)} \right\} \quad . \tag{3}$$

The drift velocity as a function of the field strength is

$$W(E) = - \frac{2}{3} \frac{eE}{m} \int \varepsilon\lambda(\varepsilon) \frac{\partial\left[F(\varepsilon)u^{-1}\right]}{\partial\varepsilon} d\varepsilon \tag{4}$$

where

$$u = \sqrt{\frac{2\varepsilon}{m}}$$

Using measured values for the mean free paths and inelasticities, they have evaluated these expressions with numerical techniques and found good agreement with the existing data. Note that in the above expressions, the mean free path $\lambda(\varepsilon) \equiv 1/N\sigma(\varepsilon)$, where N is the number of atoms per unit volume and $\sigma(\varepsilon)$ is the collision cross section. Thus λ varies inversely with the gas pressure P. This means that both the energy distribution and the drift velocity depend on the reduced field, E/P.

Drift velocities in common proportional chamber gases[5,6,7] are shown as a function of the electric field in Figures 4, 5, and 6. Argon is a common component in drift chamber gases because it has relatively high specific ionization, shows gain at moderate voltages, and shows good proportionality. It must be used with organic quenchers, however, to obtain high gain. Simple polyatomic organic molecules like CO_2 and CH_4 are photo-absorbers and so prevent the photons released in the avalanching process from initiating new avalanches. More complex organic molecules may polymerize and render a chamber inoperative if it is in a high-rate environment. As the figures indicate, the drift velocity typically increases rapidly as a function of field strength up to fields between 500 and 1000 V/cm at atmospheric pressure, at which point the velocity saturates at a value of order 5 cm/μs. Even these general properties impose some significant limitations on detector performance and design. Drift time measurements must be made with subnanosecond precision to exploit the resolution inherent in this technique. About 200 ns is required to collect the electrons from a 1 cm gap, which obviously limits the maximum rate such a chamber can handle. If the field strength in a cell is kept above the saturation field, the sensitivity of the drift time to small mechanical differences and voltage changes is minimized.

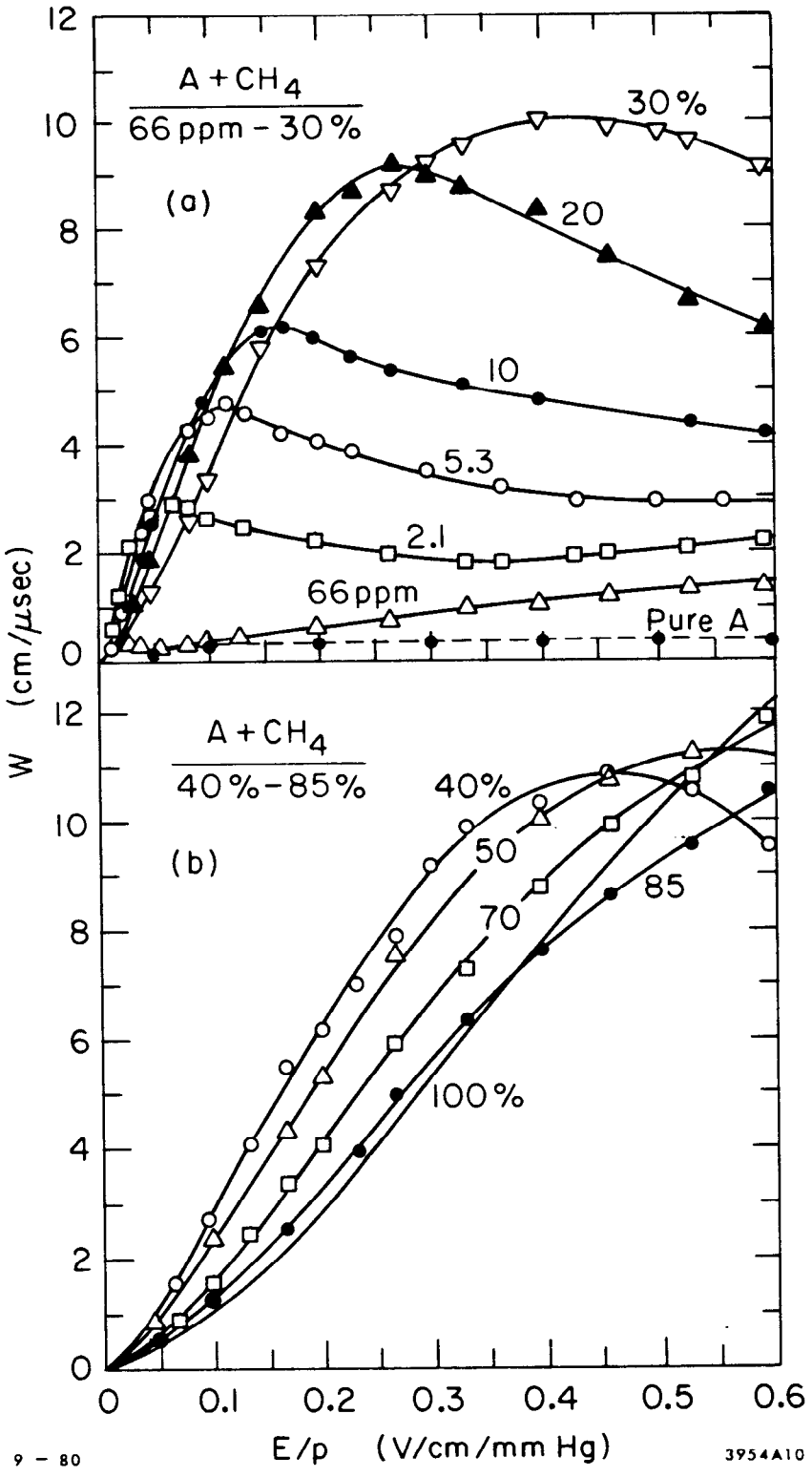

Fig. 4. Electron drift velocity in argon/methane mixtures as a function of the reduced field. Data from Ref. 5.

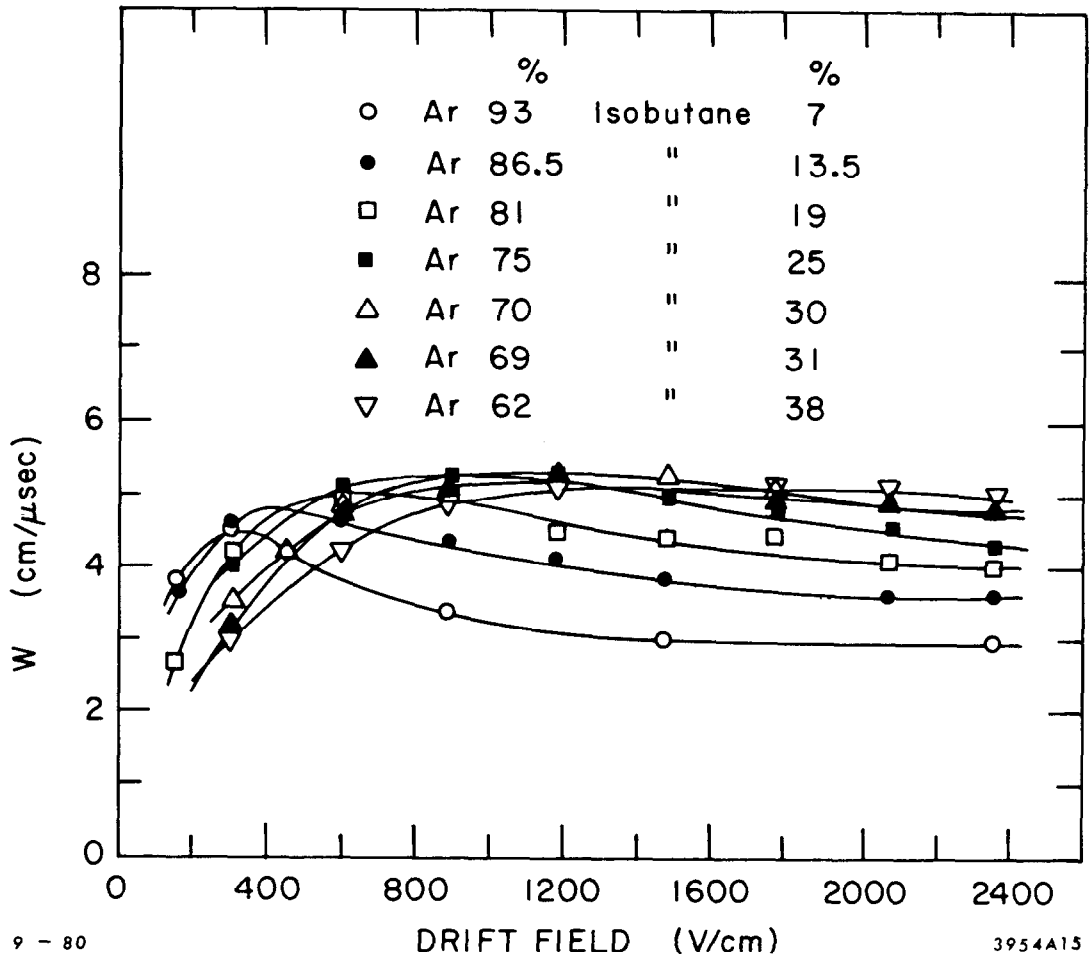

Fig. 5. Electron drift velocity in argon/isobutane mixtures as a function of electric field. Data from Ref. 6.

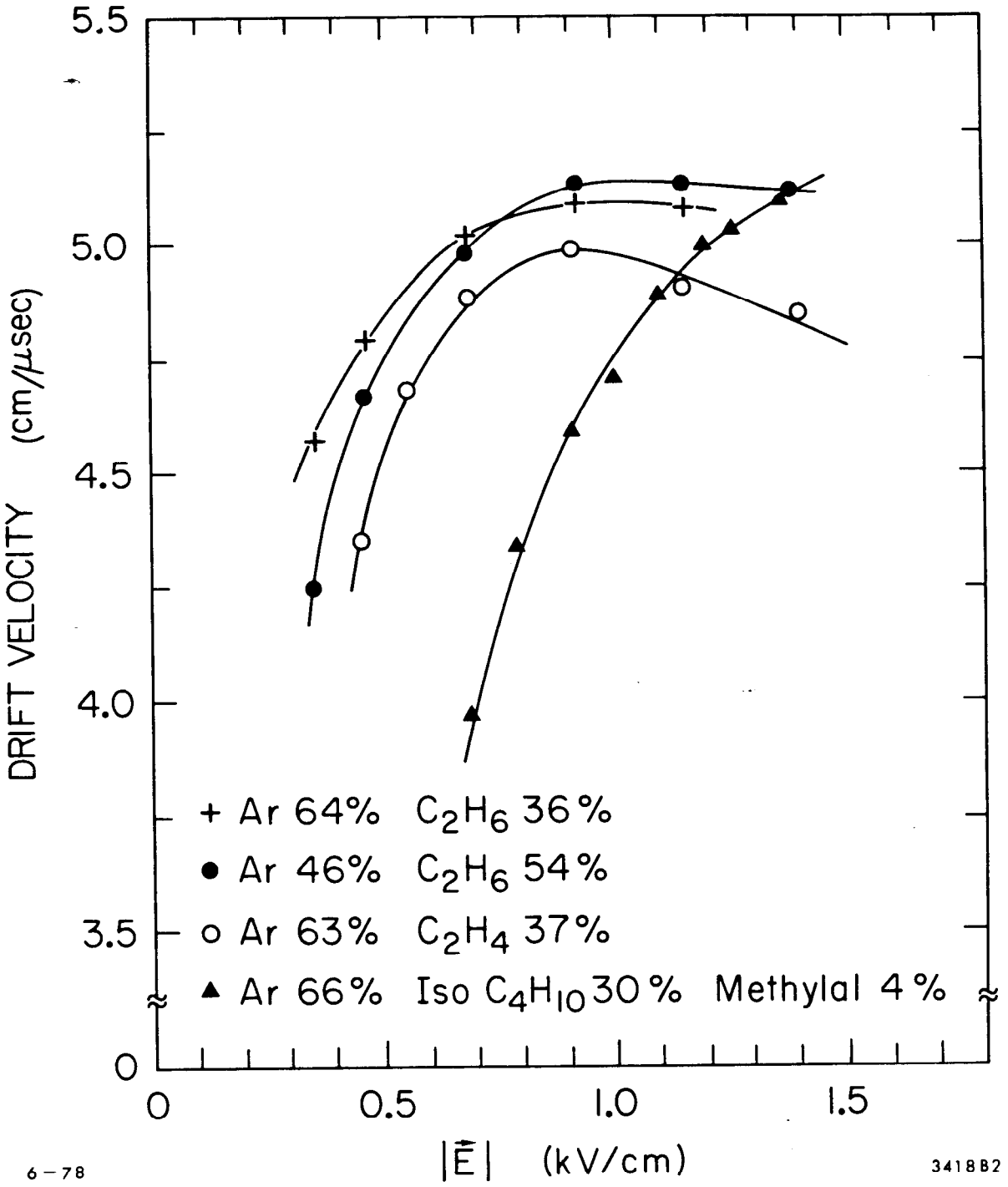

Fig. 6. Electron drift velocity in argon/ethane, argon/ethylene and argon/isobutane mixtures as a function of electric field. Data from Ref. 7.

In the presence of a 1 kV/cm electric field, an electron in an argon/ethane mixture has an average velocity near 10^8 cm/s. It collides with gas molecules every micron or so, its direction being randomized in the process. With the passage of time, the electron "random walks" away from its original location. After 200 ns of collection time it will have undergone about 2×10^5 collisions and diffused by about $1\mu \times \sqrt{2 \times 10^5} = 500\mu$. More precisely, the diffusion transverse to the direction of drift is given in terms of the diffusion constant D and the drift time t as

$$\sigma_T = \sqrt{2Dt} \quad . \tag{5}$$

The diffusion coefficient D is given in terms of the electron energy distribution as

$$D = \frac{1}{3} \int u \, \lambda(\varepsilon) \, F(\varepsilon) \, d\varepsilon \quad , \tag{6}$$

and so is an implicit function of (E/p). Figure 7 gives the root-mean-square of the transverse diffusion after 1 cm of drift for various gases[8] as a function of field strength. Pure argon, with its anomalously low-drift velocity, has $\sigma_T \sim 1000\,\mu$. In the common argon/isobutane 70/30 mixture, σ_T is comparable to pure CH_4, about $250\,\mu$.

The resolution achievable with drift time measurements clearly depends upon electron diffusion and the particular strategy employed in detecting the ionization (e.g., low threshold vs. center of ionization). It has recently been appreciated that longitudinal diffusion, i.e., diffusion in the direction of the drift velocity, is not equal to the transverse diffusion. In fact, as data in pure argon[9] and the data[10] in Figure 8 show, the coefficient of longitudinal diffusion is about a factor of 4 smaller than that for transverse diffusion. Measurements of

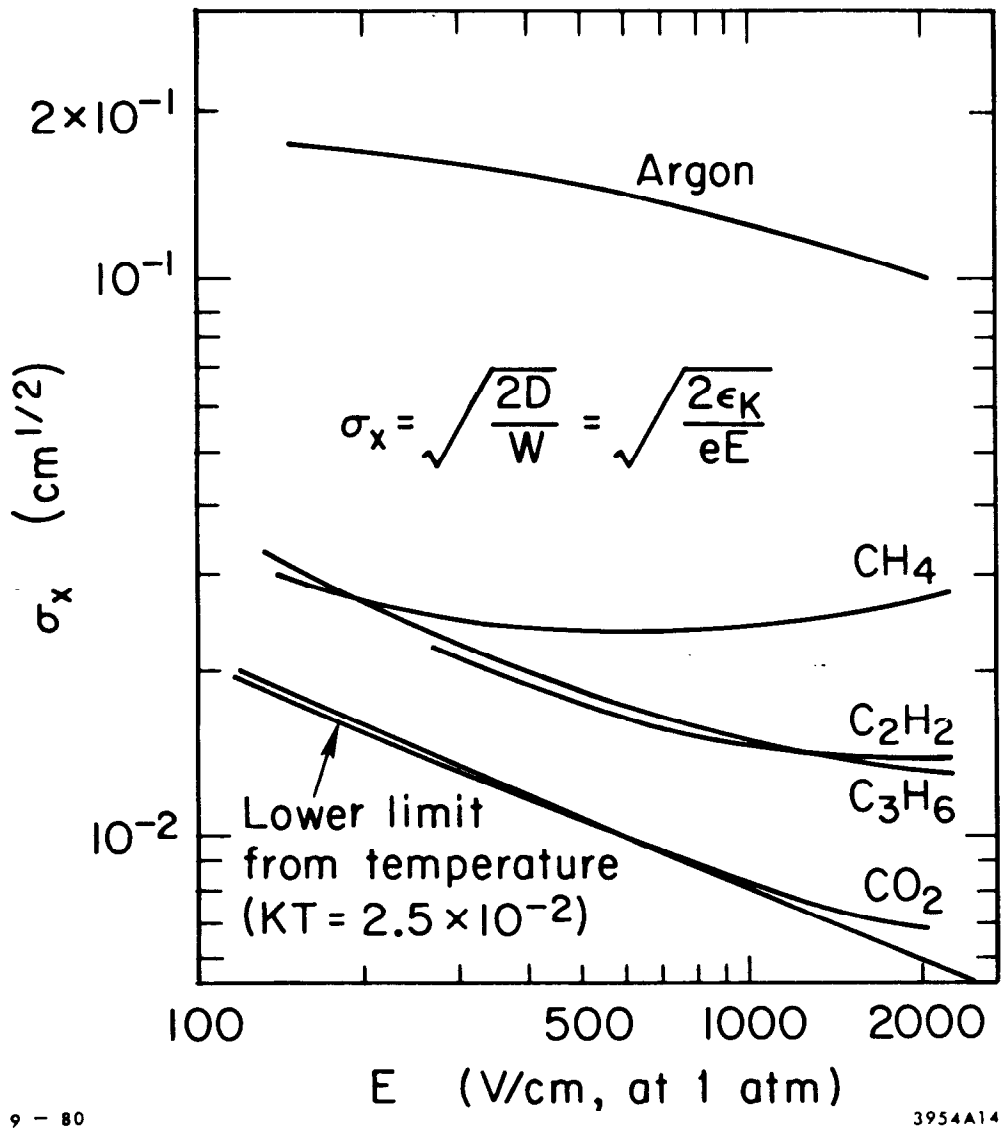

Fig. 7. Spatial resolution due to transverse diffusion after 1 cm drift as a function of the electric field in various gases. Data from Ref. 8.

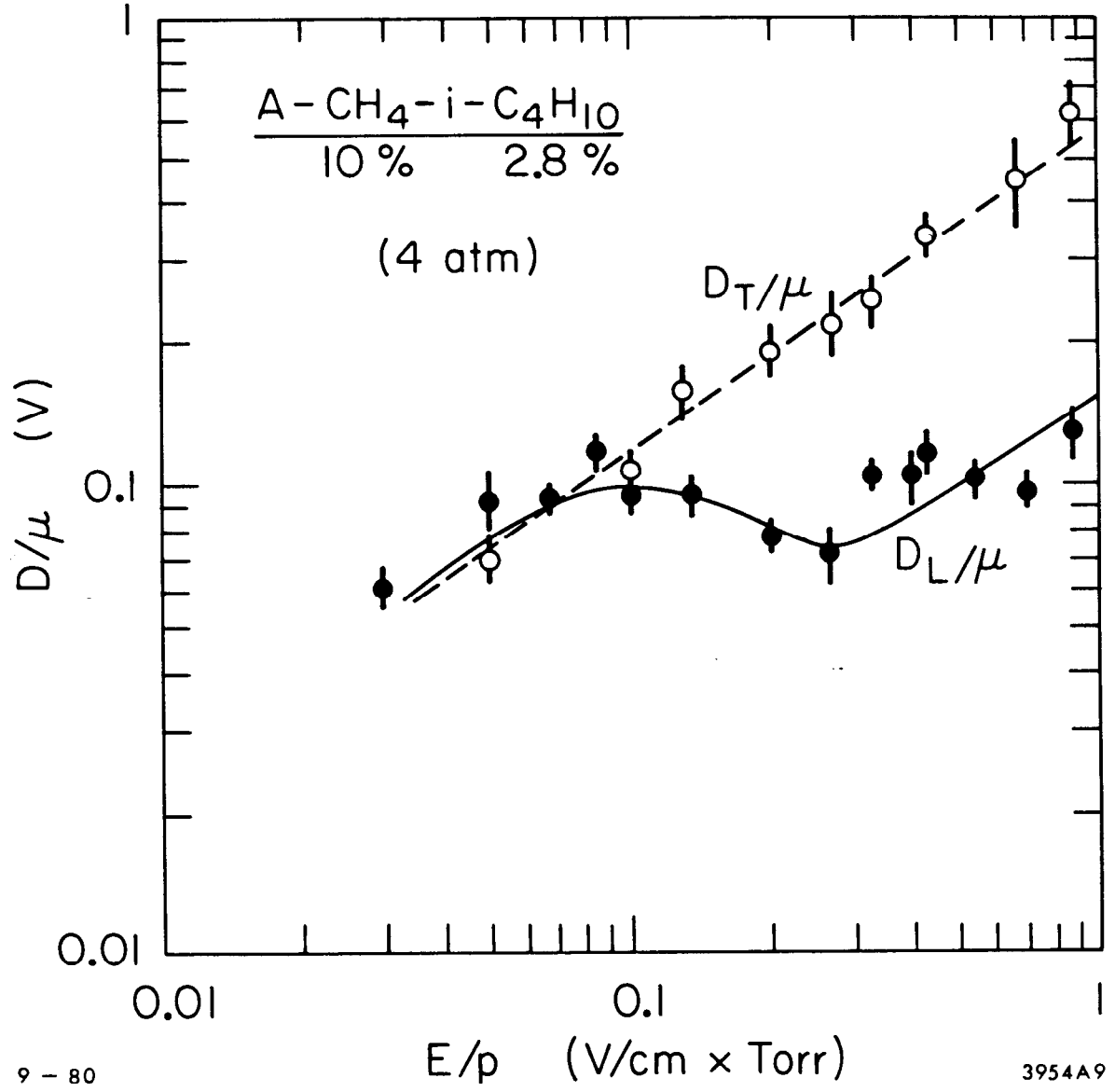

Fig. 8. Coefficients of longitudinal and transverse diffusion as a function of the reduced field. Data from Ref. 10.

longitudinal diffusion have not been made in many proportional chamber gases as yet, so we shall adopt the rule of thumb $\sigma_L = \sigma_T/2$ as a guide in evaluating diffusion effects in drift chambers. Then, we expect the spatial resolution after 1 cm of drift to be limited to ~ 100 μ in argon/isobutane mixtures at one atmosphere. To do substantially better than this, one must increase the pressure or use other gases. Notice that the diffusion constant D varies inversely with the pressure; thus increasing the pressure reduces the diffusion. D also depends on the average electron temperature in the gas. Thus a "cool" gas, like pure isobutane, has considerably lower diffusion than the more common argon/isobutane mixtures. Figure 9 illustrates these points. Note that even over the smallest practical drift distances (~ 1 mm), diffusion significantly limits the resolution inherent in a drift time measurement. For a given permissible resolution, it limits the maximum drift distance unless a new measurement strategy is adopted. Two such techniques should be mentioned. By timing the center of gravity of an n-electron bunch instead of the arrival of the first electron, one could hope to reduce the diffusion by a factor $1/\sqrt{n}$. In practice, this full reduction isn't realized unless the drift-length differences among the electrons are smaller than the expected diffusion. The other technique is to arrange the drift field parallel to an intense magnetic field. In the appropriate gas, this can limit transverse diffusion by forcing the drifting electrons into tight helical paths. Jay Marks' lecture[11] gives the details of this scheme.

The effect of magnetic fields on electron collection in a drift chamber is important in many applications. Chambers have been operated in moderately high magnetic fields (15 kG) with success. Here we shall consider the common situation where $\bar{E}$ and $\bar{B}$ are perpendicular. In this

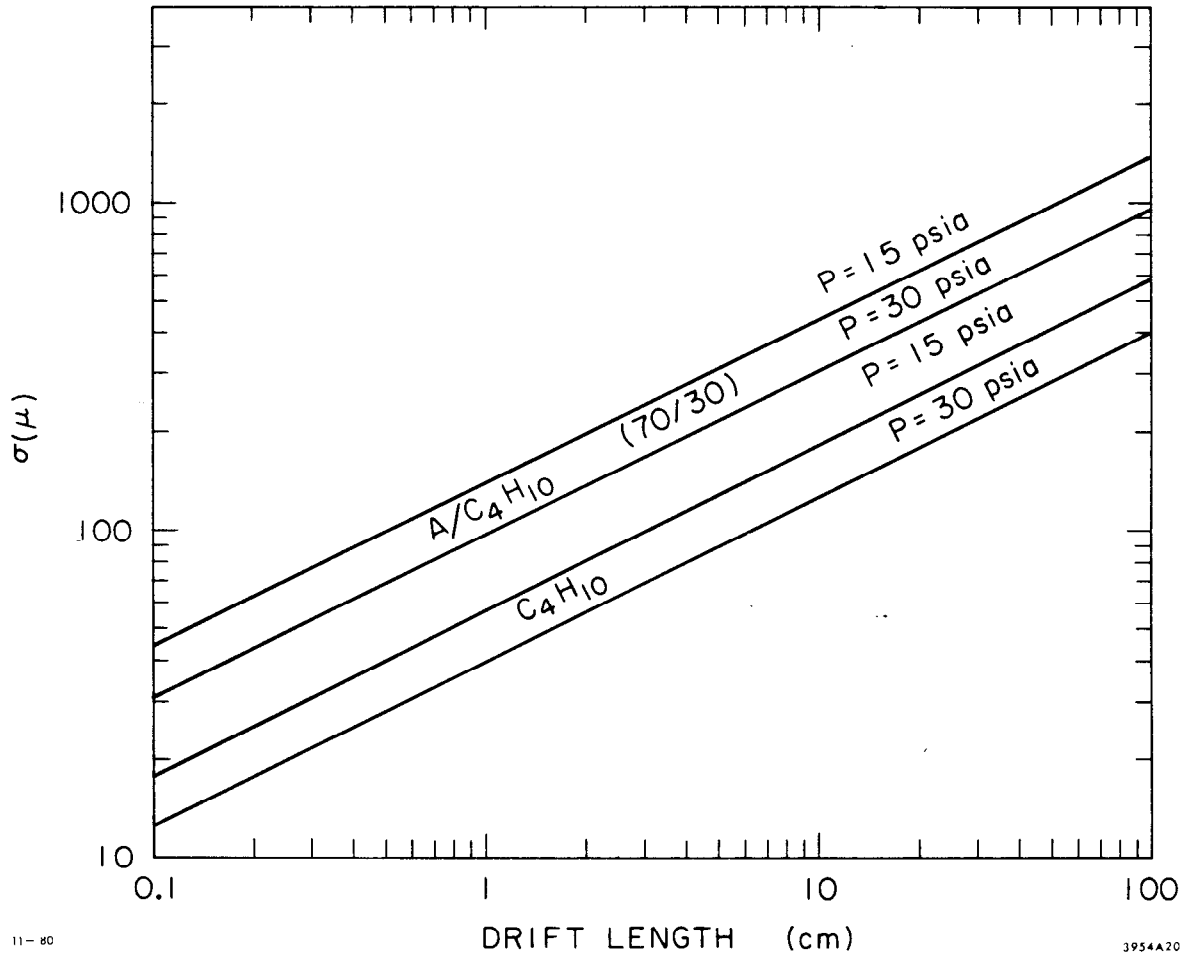

Fig. 9. Spatial resolution due to longitudinal diffusion as a function of drift length in argon/isobutane and in pure isobutane at 1 and 2 atmospheres pressure..

case, there are two effects: (1) the electrons drift at an angle θ with respect to the local electric field direction; (2) the drift velocity is reduced. Figures 10 and 11 illustrate these effects in argon/isobutane/methylal.[12] Notice that the Lorentz angle θ becomes large at high field strengths; argon/xenon mixtures have angles about half those of argon-isobutane and may be useful in very high magnetic fields. As Figure 11 shows, increasing the magnetic field at moderate electric fields decreases the drift velocity. At high electric fields, however, the effect is negligible.

The dependence of the drift angle and drift velocity on the field strengths can be parameterized in terms of two gas-dependent constants, K_1 and K_2, the Larmor frequency $\omega = eB/m_e c$, and the mean time between collisions, τ. Following Reference 13, we write

$$\tau = K_1 \, m_e W_0 / eB \qquad (7)$$

$$\theta = \arctan \left\{ K_2 \, \frac{B}{E} \, \frac{W_0}{\left(1 + \omega^2 \tau^2\right)^{\frac{1}{2}}} \right\} \qquad (8)$$

and

$$\bar{W} \cdot \bar{E} = W_0 \Big/ \left(1 + \omega^2 \tau^2\right) \quad . \qquad (9)$$

W_0 is the drift velocity in vanishing magnetic field, and the constants K_1 and K_2 are about 5 for a 90/10 argon/methane gas mixture.

Figure 12, also from Reference 13, shows rather dramatically how a high magnetic field warps the "electron-geodesics". Families of electron trajectories have been drawn for the case where $B = 0$ (Figure 12(a)) and where $B = 15$ kG (Figure 12(b)). In the high field case, the space-time relation is strongly angle-dependent and left-right asymmetric. To avoid such complexities, several groups have built chambers like the one shown schematically in Figure 1(e). In these

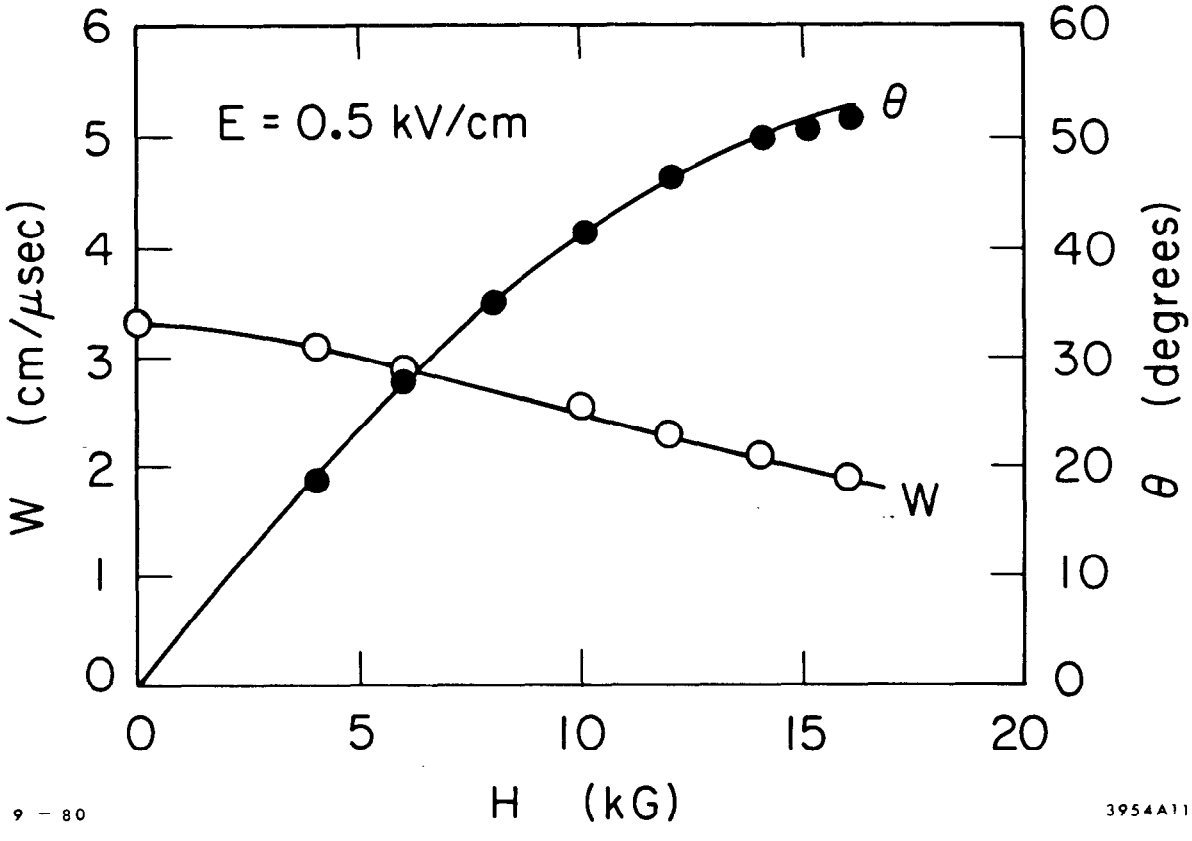

Fig. 10. Dependence of the drift velocity and the Lorentz angle on magnetic field in argon/isobutane at .5 kV/cm. Data from Ref. 12.

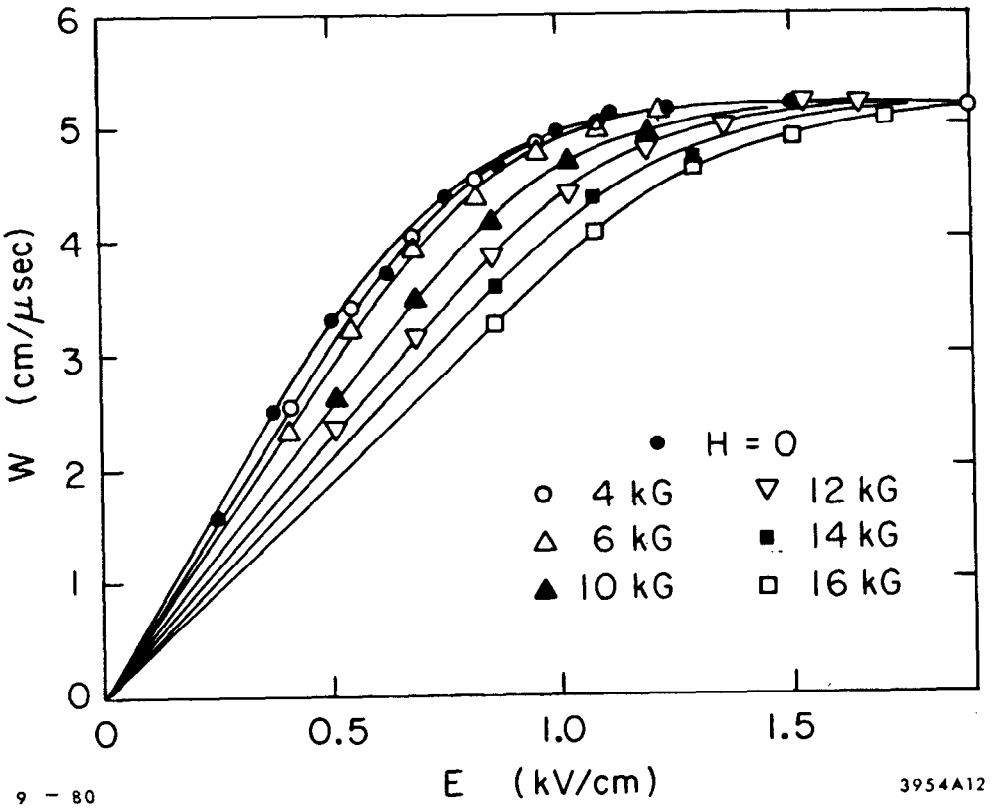

Fig. 11. Dependence of the drift velocity on the electric field for different magnetic fields. Data from Ref. 12.

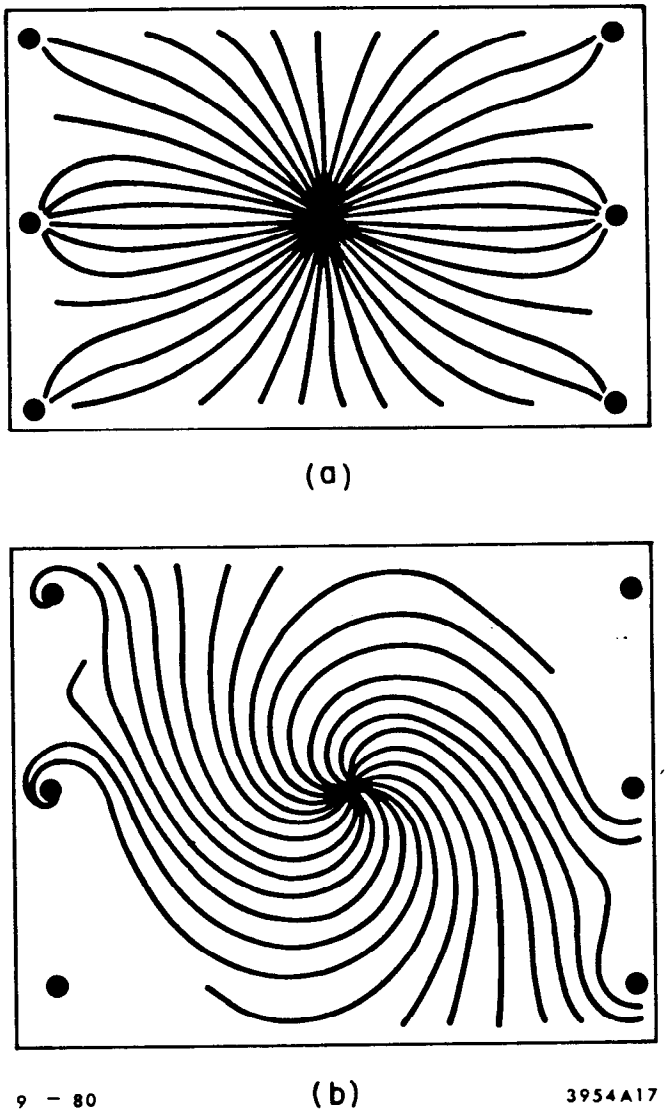

Fig. 12. Electron drift trajectories in the CELLO drift cell with (a) B = 0 and (b) B = 15 kG. Data from Ref. 14.

chambers, the electric field is uniform over much of the active area. Then the electron trajectories are straight lines, tilted with respect to the electric field direction.

IV. AMPLIFICATION AND PULSE FORMATION

Within about 100 μ of the anode wire, the local electric fields are so intense that electrons are accelerated to energies great enough to ionize gas molecules. This frees more electrons, and the process cascades, multiplying the initial 30 or so electrons by a factor of order 10^5 in a typical drift chamber. The process is described in terms of the first Townsend coefficient, α, which is the number of ion pairs produced per centimeter of travel. The amplification factor A can be written

$$A = e^{-\int \alpha(r) dr} \quad , \tag{10}$$

where the integration is over the electron path length. As long as space-charge effects are small, the amplification factor is the same for all the collected electrons. Hence the chamber response is proportional to the amount of initial ionization. Figure 13 shows the first Townsend coefficient as a function of the reduced field in the noble gases.[14] Electric fields near the anode wire are typically in the range $|\vec{E}| = 4000\ (\text{kV/cm})/r(\mu)$; in the amplification region the mean free path for an ionizing collision ranges from about 10 μ to 1 μ, comparable to the classical mean free path for an electron in a gas.

The Rose-Korff parameterization[15] is a handy guide to the rough magnitude of the amplification in a proportional chamber. It is given in terms of the chamber parameters (the voltage V, the anode wire radius r_a, and the wire capacitance per unit length C) and the gas parameters (the rate of change of the ionization cross section with

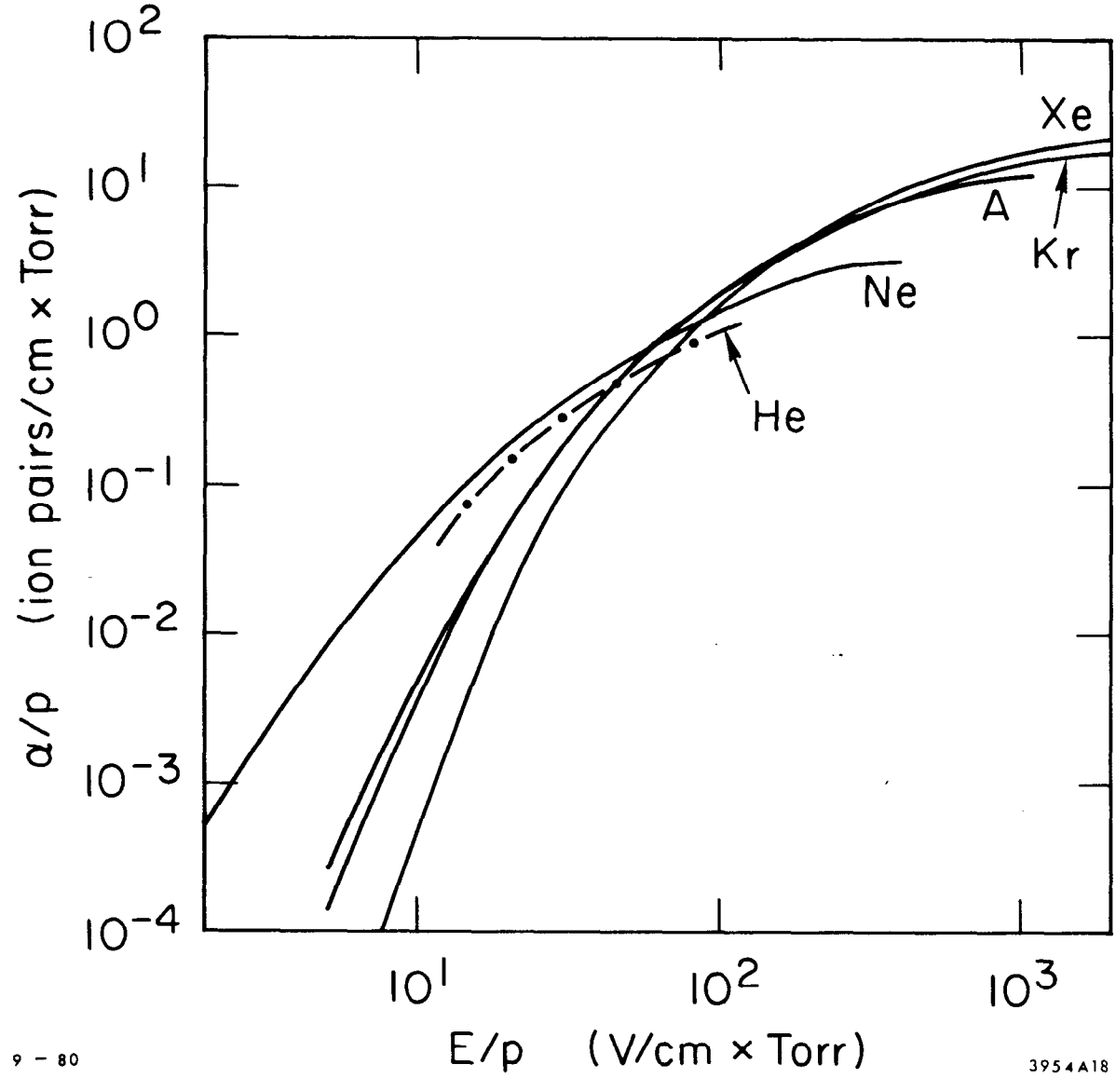

Fig. 13. Dependence of the first Townsend coefficient on the reduced field for the noble gases. Data from Ref. 14.

energy a, the number of gas molecules per unit volume N, and the voltage at which amplification begins, V_T) as follows:

$$A = \exp\left\{2\sqrt{aNCr_a V}\left(\sqrt{\frac{V}{V_T}} - 1\right)\right\} \quad . \tag{11}$$

V_T is treated as a free parameter and determined by fitting the behavior of the amplification at low voltage. When $V >> V_T$, the amplification is seen to depend roughly exponentially on the chamber voltage; a typical chamber gain doubles in about 150 V. Gains up to 10^5 are common in practice and give rise to signals of order 1 mV/electron. This sets the required level of electronic sensitivity for the detection of single electrons. Higher gains have been achieved in certain gas mixtures, but space-charge effects limit the proportional amplification regime to gains $\lesssim 10^5$.

Amplification is of course a statistical process, so wide variations in the pulse height are expected when single electrons are detected. Curran, Cockroft and Angus[16] have found that the distribution of amplification obeys

$$P(\eta) = \frac{3}{2}\eta \exp\left\{-\frac{3}{2}\eta\right\} \tag{12}$$

where

$$\eta = \frac{A}{\bar{A}} \quad .$$

This distribution is shown in Figure 14; its variance is large, $\sigma_A = \sqrt{\frac{2}{3}}\,\bar{A}$. Such wide variations in the pulse height from a single electron can cause substantial time slewing in the detecting electronics. The mean pulse height must be considerably above the electronic threshold to achieve good timing resolution. Although the pulse height variations from single electrons are large, the variations seen in a typical chamber

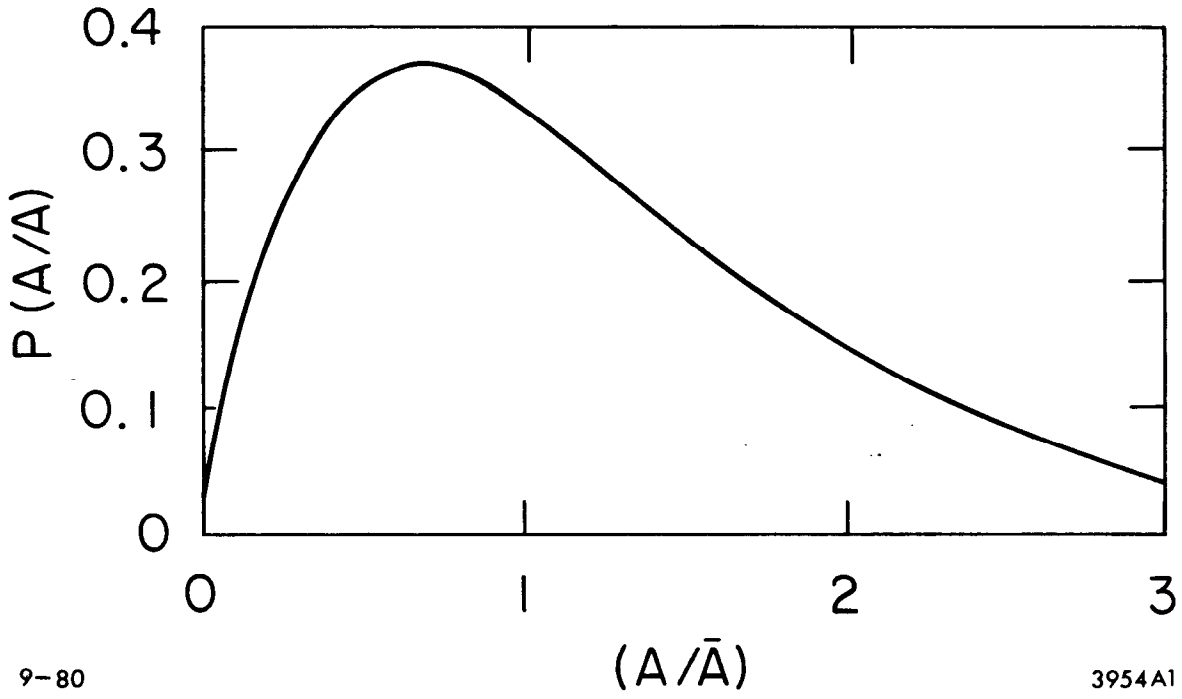

Fig. 14. Distribution of the amplitude of proportional chamber pulses from a single electron.

(where perhaps 30 electrons are collected) are dominated by the ionization statistics, not the amplification process. Letting $\bar{m}$ be the average number of primary electrons and σ_m its dispersion, the net dispersion σ is given by[17]

$$\frac{\sigma^2}{(\bar{m}\bar{A})^2} = \frac{\sigma_m^2}{\bar{m}^2} + \frac{2}{3\bar{m}} \quad . \tag{13}$$

The second term comes from variations in the amplification.

The pulse observed on the anode wire of a proportional chamber is induced by the motion of the charges released in the avalanche. The motion of the positive ions contributes most of the observed pulse. The voltage induced as a function of time is

$$V_+(t) = -\frac{Q}{\ell} \ln\left(1 + \frac{t}{t_0}\right) \quad , \tag{14}$$

where

$$t_0 = \frac{r_a^2 P}{4\mu^+ CV} \quad .$$

Here Q is the total charge of the ions, P the pressure, ℓ the anode wire length, and μ^+ the mobility of the positive ions. The pulse has a very rapid rise followed by a slow logarithmic approach to its maximum value, $-Q/\ell C$, which occurs when the positive ions have been collected at the cathode. This occurs at a time $t = P(r_b^2/r_a^2 - 1)t_0$, where r_b is the radius of the cathode surface. Figure 15 shows V/V_{max} as a function of time. A typical chamber has $t_0 = .5$ ns and a total collection time in the 1 ms range. Notice that about 20% of the signal appears within a few nanoseconds of the avalanche time.

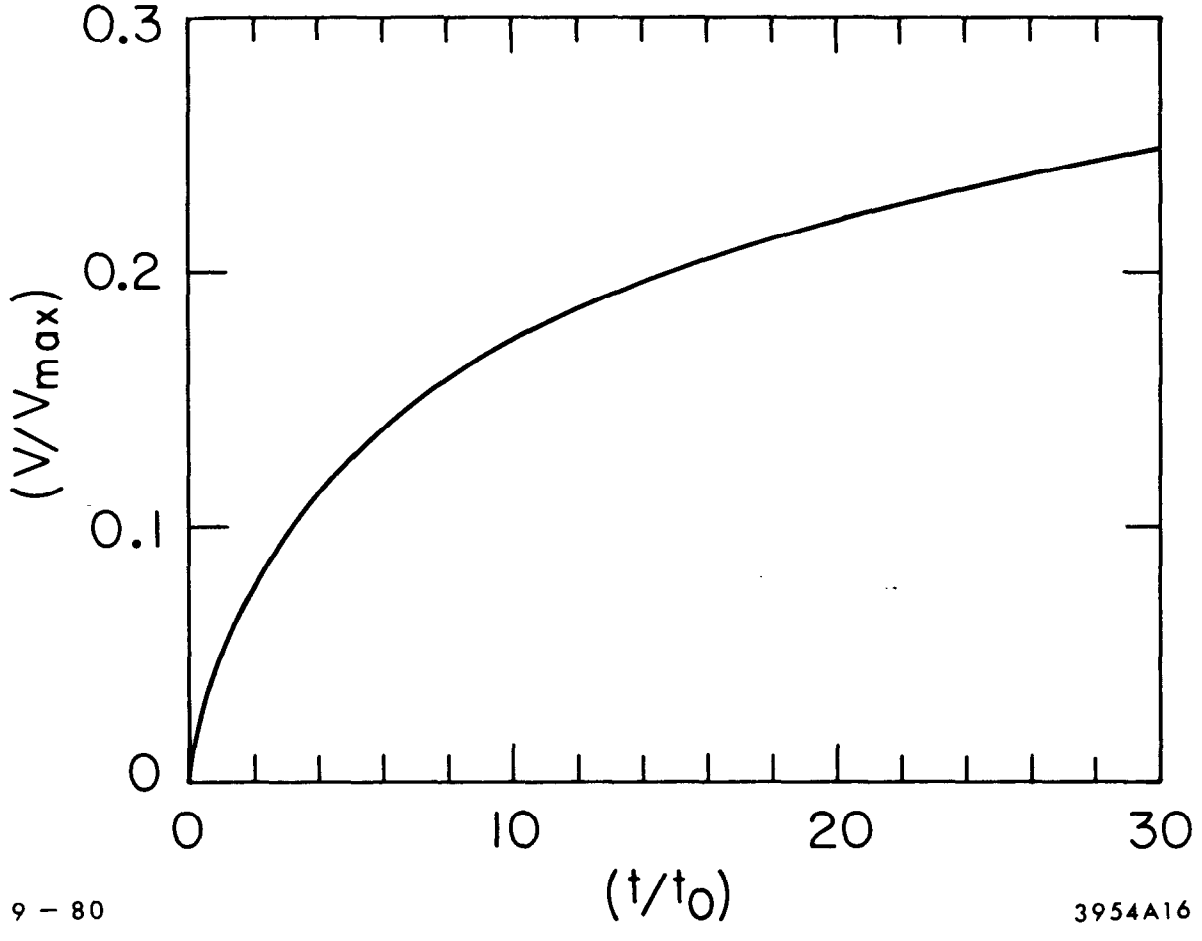

Fig. 15. Time development of a proportional chamber signal.

The expression for $V_+(t)$ applies to the case of arbitrarily high amplifier input impedance; in practice the input impedance is in the 1 KΩ range, which coupled to a typical wire capacitance gives RC' between 10 and 100 ns. The result is the sharp differentiation of the input pulse. The maximum in the differentiated signal appears at $t \approx RC'$ and has a relative amplitude[18]

$$\frac{V}{V_{max}} = \left(\frac{RC'}{t_{col}}\right) \frac{r_b^2/r_a^2}{2 \log\left(r_b/r_a\right)} \quad . \tag{15}$$

The resulting pulses typically have widths in the 10-100 ns range and pulse heights of order 10-40% of V_{max}. This pulse width of course imposes rate limitations for each wire, and the pulse height loss due to differentiation means that a threshold of order 300 μV is required to see a single electron. Since the rise time of the differentiated pulse is in the few nanosecond range, the electronic rise-times should be comparable so as not to introduce excessive slewing.

V. PERFORMANCE LIMITATIONS IN DRIFT CHAMBERS

High rate capability, good track-pair resolution, and good spatial resolution are the key requirements for tracking chambers in the newly completed or soon-to-be completed colliding beam devices. Rate limitations come about from at least two considerations. The width of the output pulse depends on how sharply the chamber output has been differentiated and on the range of electron arrival times. The width is typically 100 ns and so imposes an upper limit of about 2 MHz per wire. At such high rates, space charge effects become important for chambers operated at gains $\geq 10^5$. The sheath of positive ions migrating away from the anode wire lowers the fields seen by incoming electrons and

so reduces the amplification. Breskin et al.,[19] found that wires grew inefficient at rates greater than a few megahertz per meter of wire length.

Track-pair resolution depends of course on the geometry of the drift-cell and the capabilities of the electronics. In simple single-hit cells, the resolution is roughly given by the cell size. Systems with redundant cells offset from one another can obviously do better, but the current practical limit is about 1 cm. Information from two tracks separated by less than this amount is lost. With larger drift spaces and multi-hit electronics, the limit to track-pair resolution comes from the width of the output pulse associated with one track. In the Jade detector at PETRA, a track-pair resolution of 5 mm has been achieved,[20] and in a prototype device, the Charpak group[21] has achieved about 2.5 mm. The corresponding pulse widths are 100 and 50 ns, respectively, very near the limit imposed by the drift-time differences associated with any track.

The fundamental limits to spatial resolution have not been so closely approached. As we have discussed above, the statistical nature of the ionization process and the diffusion of the electrons during the collection time contribute significantly to the spatial resolution. Increasing the gas pressure and choosing a "cool" gas can lead to significant improvements in the resolution as indicated in Figure 16. This technique has been demonstrated by a Heidelberg group,[22] whose data is shown in Figure 17. We have obtained similar results in argon/ethane (50/50) and argon/isobutane (70/30) mixes (Figure 18) for a drift of a few millimeters.

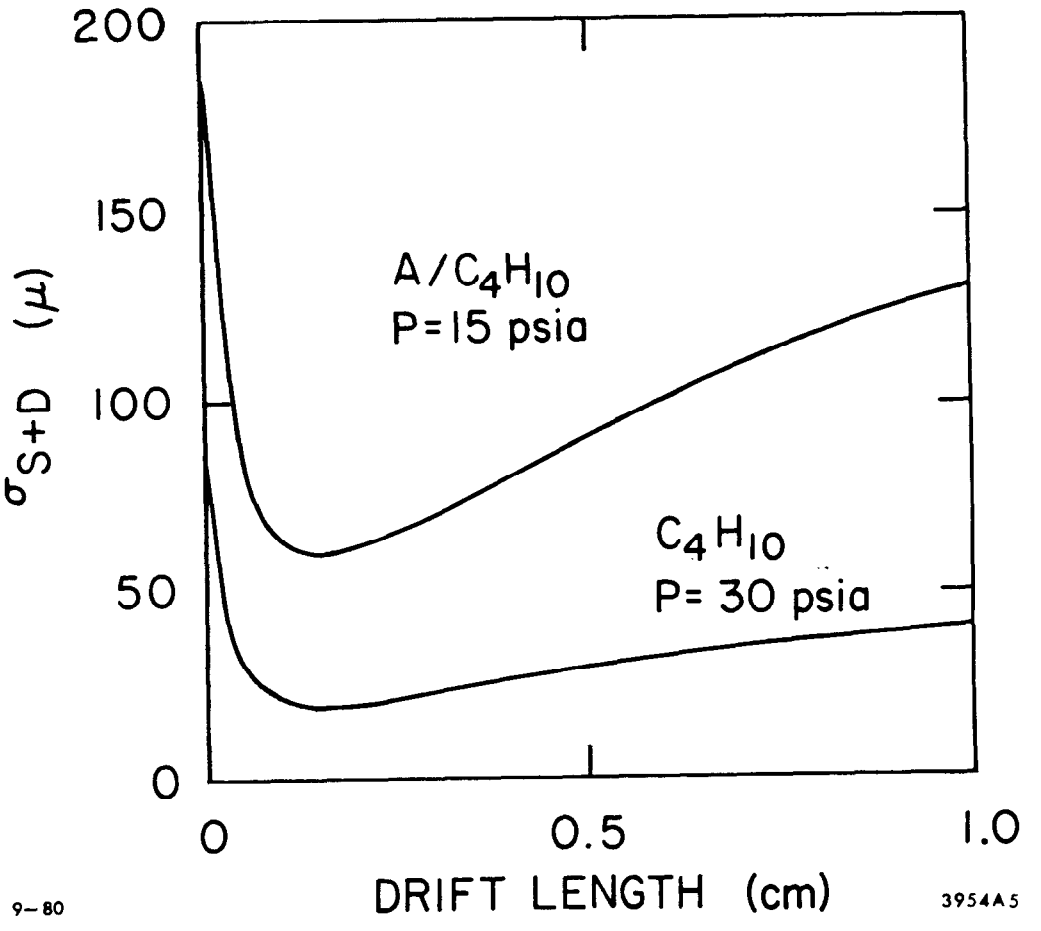

Fig. 16. Spatial resolution due to ionization statistics and diffusion as a function of drift length in different gases.

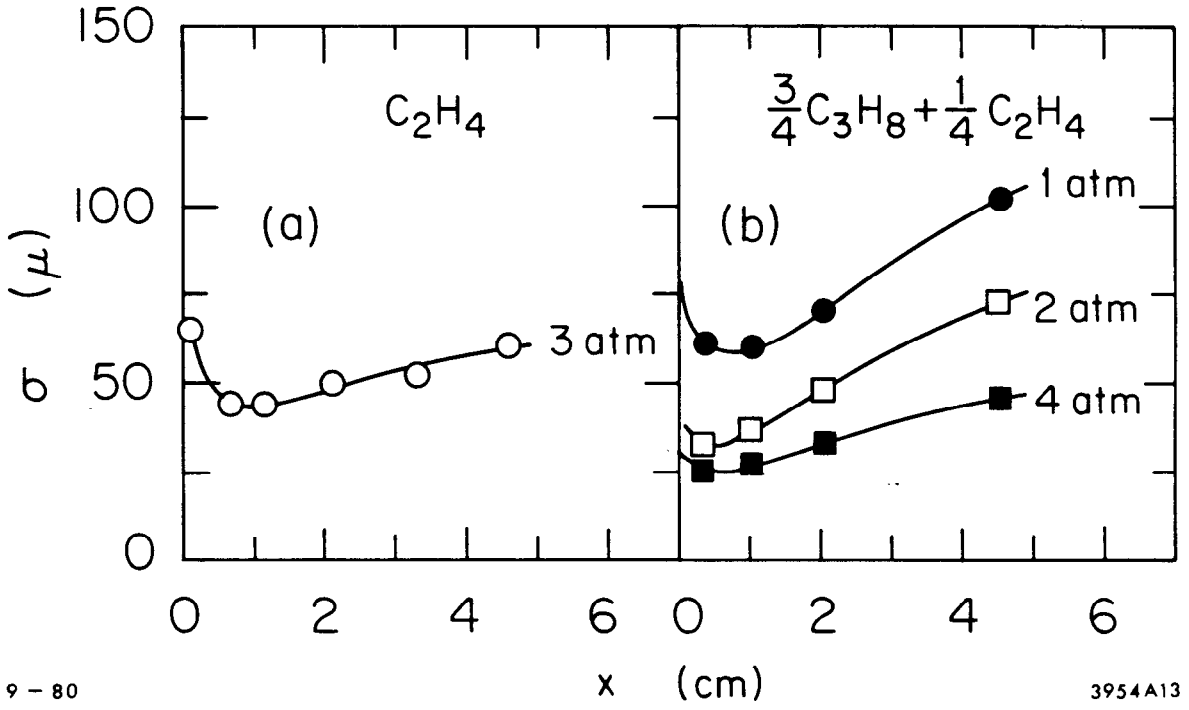

Fig. 17. Measured spatial resolution as a function of drift distance in organic gases at several pressures. Data from Ref. 22.

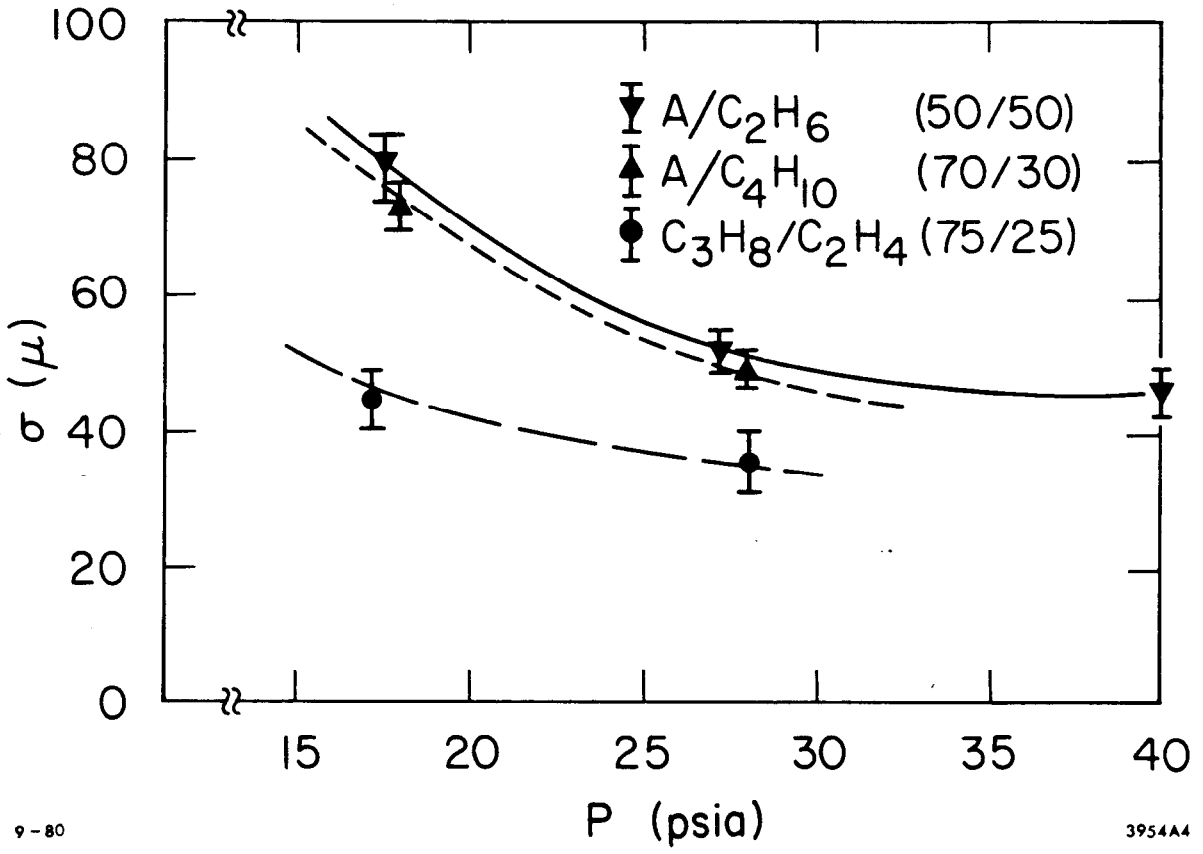

Fig. 18. Measured spatial resolution as a function of gas pressure in several gases for 3 mm drift length.

Spatial resolution depends rather critically on electronic threshold sensitivity. For a fixed threshold, the resolution improves dramatically with increased chamber gain, and only saturates hundreds of volts beyond the beginning of the efficiency plateau, at least for drift lengths $\leq$ 1 cm. For longer drift distances, where a large number of electrons arrive at the anode at nearly equal times, diffusion effects can be reduced by measuring the arrival time of the nth electron. We have modeled this situation with Monte Carlo techniques with the following assumptions: (1) cylindrical electric field; (2) drift velocity independent of the field; (3) thirty ion pairs produced per centimeter; (4) $\sigma_{DIFF} = 100\mu \times \sqrt{x(cm)}$. Figure 19 shows the spatial resolution as a function of drift length for thresholds corresponding to one, two and four electrons. Pulse height variations and rise-time effects have been ignored, so the graph should only be taken as a rough guide. Still, it indicates the importance of sensitive electronics for the measurement of drifts under 1 cm. Figure 20 shows the improvement in the resolution for short drift lengths that we have observed in propane/ethylene (75/25) as high voltage has been increased beyond the beginning of the efficiency plateau. Resolution improves as the gain increases.

Achieving high spatial resolution in a drift chamber system with a large number of wires requires that considerable attention be paid to many details. Some of these are listed in Table 2 for a high resolution system we have proposed. Sources of error include the mechanical precision in wire placement; timing uncertainties and time-measurement inaccuracies; variations in gas pressure and temperature and chamber voltage; and the more fundamental limitations we have discussed above. Taking these errors into account, it should be possible

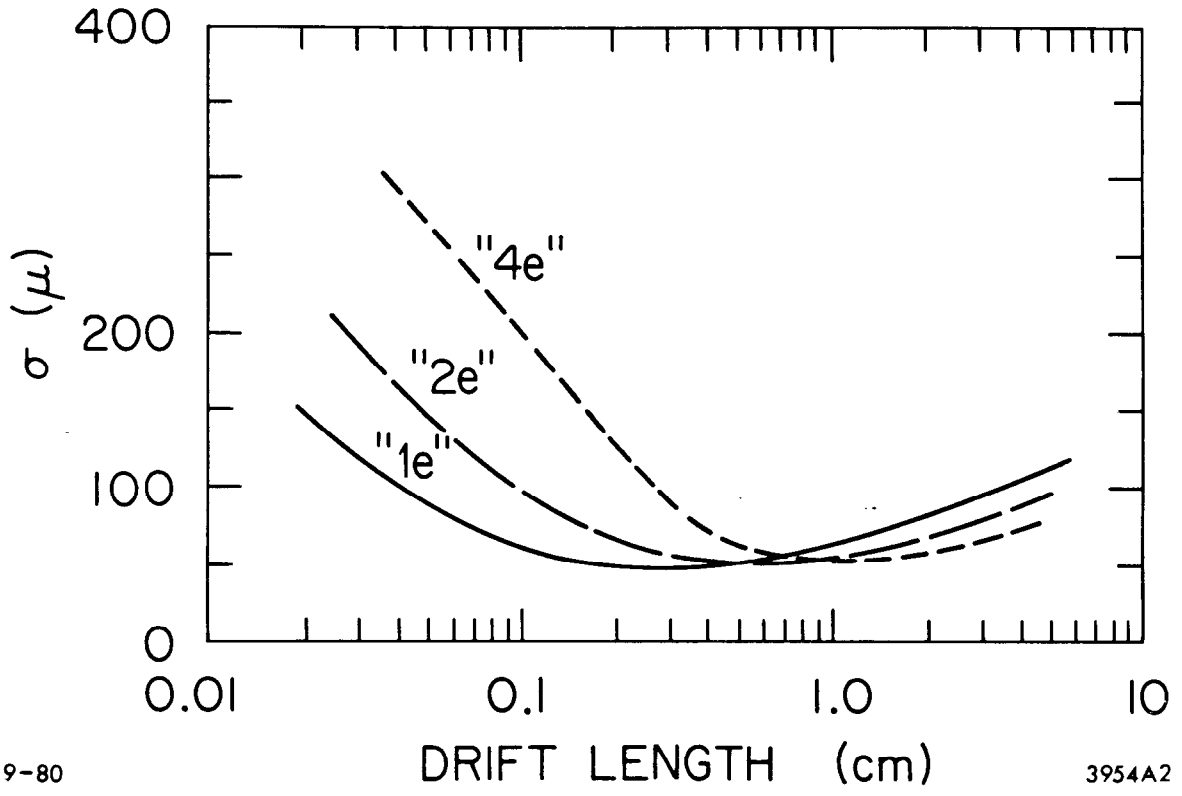

Fig. 19. Modeled dependence of spatial resolution on drift length for various threshold sensitivities.

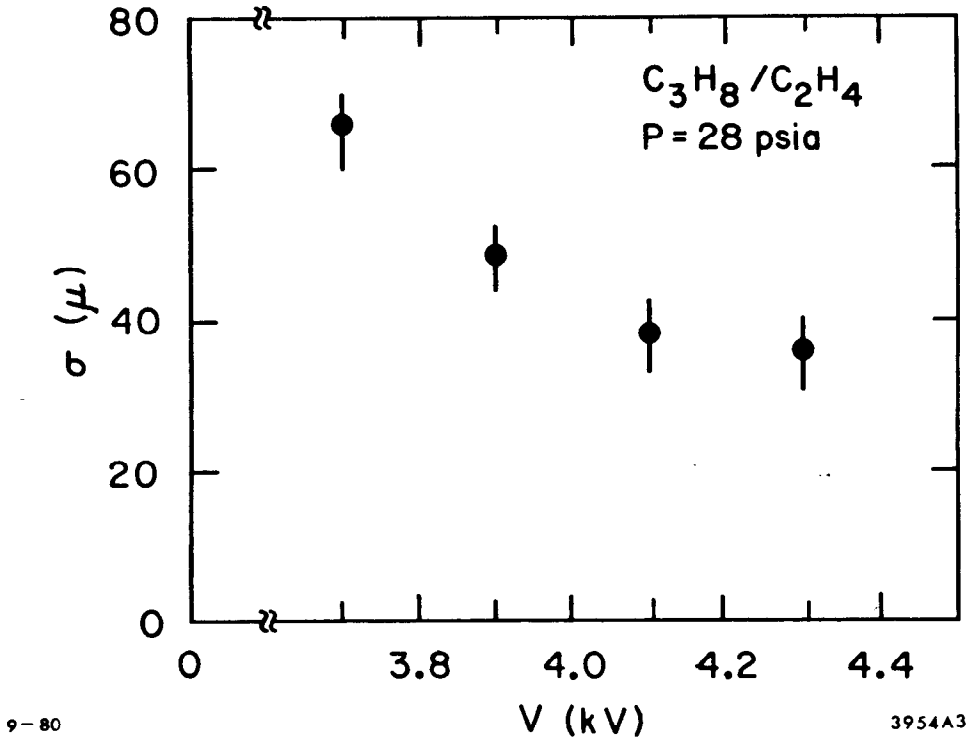

Fig. 20. Measured spatial resolution in propane/ethylene as a function of high voltage.

TABLE 2

	$\sigma(\mu)$
I. MECHANICAL TOLERANCES	
Wire Placement	10
Gravitational Sag (40 μ, corrected knowing Z and tension)	5
Electrostatic Displacement	5
	12
II. TIMING UNCERTAINTIES	
Start-Time (.2 ns)	10
Particle Time-of-Flight to Layer (.1 ns)	5
Signal Propagation (.1 ns, knowing Z)	5
TDC Calibration (.1 ns)	5
TDC Resolution (.2 ns)	10
	17
III. CHAMBER PARAMETERS	
High Voltage Variation (10 V)	10
Temperature Changes (1° C)	10
Pressure Changes (.1 PSI)	10
Cell-to-Cell Gain Variations	5
	18
IV. DRIFT-TIME ACCURACY	
Intrinsic Resolution	40
Space-Time Relationship Uncertainty	20
	45

OPTIMAL SYSTEM RESOLUTION: 50 to 55 μ

using present techniques to construct systems with spatial resolutions in the 50 μ range, i.e., markedly below the 200 μ common to most big systems today.

VI. CONCLUSIONS

Tracking chambers based on drift-time measurements in proportional counters have demonstrated good time, track-pair, and spatial resolution. Diffusion, the statistics of ion formation, and electronic timing jitter limit the spatial resolution to 100-200 μ; by using pressurized gases and operating the chamber well beyond its efficiency threshold, resolutions in the range 25 - 50μ are possible. Even with such improvements, the spatial resolution is more than an order of magnitude worse than that inherent in the ionization process in a gas.

ACKNOWLEDGMENT

It is a pleasure to thank David Ritson and Jay Marks for useful discussions.

REFERENCES

1. G. Charpak, "Evolution of the Automatic Spark Chamber," Ann. Rev. Nuclear Sci. 20, 195 (1970).

2. F. Sauli, "Principles of Operation of Multiwire Proportional and Drift Chambers," CERN report 77-09 (1977).

3. V. Palladino and B. Sadoulet, Nuc. Instru. and Meth. 128, 323 (1975).

4. D. Ritson, talk at this Institute.

5. H. W. Fulbright, "Ionization Chambers in Nuclear Physics," Encyclopedia of Physics, S. Flügge, ed., Springer-Verlag, Berlin, 1958, p. 1.

6. A. Breskin, et al., Nuc. Instr. and Meth. 160, 227 (1975).

7. W. Davies-White, et al., Nuc. Instr. and Meth. 160, 227 (1975).

8. V. Palladino and B. Sadoulet, op. cit.

9. J. J. Lowke and J. H. Parker, Phys. Rev. 181, 302 (1960).

10. A. Wagner et al., "Experience with the Jet-Chamber of the Jade Detector at PETRA," in Proceedings of the Wire Chamber Conference, Vienna, 1980, to be published in Nucl. Inst. and Meth.

11. J. Marks, talk at this Institute.

12. A. Breskin et al., op. cit.

13. W. de Boer et al., "Behavior of Large Cylindrical Drift Chambers in a Superconducting Solenoid," in Proceedings of the Wire Chamber Conference, Vienna, 1980, to be published in Nucl. Inst. and Meth.

14. S. C. Brown, Basic Data of Plasma Physics, MIT Press, Cambridge, Mass., 1959.

15. M. E. Rose and S. A. Korff, Phys. Rev. 59, 850 (1941).

16. S. C. Curran, A. L. Cockroft and J. Angus, Phil. Mag. 40, 929 (1949).

17. D. H. Wilkinson, Ionization Chambers and Counters, Cambridge University Press, 1950, p. 143.

18. D. H. Wilkinson, op. cit.

19. A. Breskin et al., op. cit.

20. A. Wagner, op. cit.

21. A. Breskin et al., op. cit.

22. W. Farr et al., Nucl. Instr. and Meth. 154, 175 (1978).